

***In vivo* analysis of THz wave irradiation induced acute inflammatory response in skin by laser-scanning confocal microscopy**

Yoonha Hwang,¹ Jinhyo Ahn,¹ Jungho Mun,² Sangyoon Bae,² Young Uk Jeong,²
Nikolay A. Vinokurov,² and Pilhan Kim^{1,*}

¹Graduate School of Nanoscience and technology, Korea Advanced Institute of Science and Technology (KAIST),
Daehak-ro 291, Yuseong-gu, Daejeon, 305-701, South Korea
²Center for Quantum-Beam-based Radiation Research, Korea Atomic Energy Research Institute (KAERI), Daedeok-
daero 989-111, Yuseong-gu, Daejeon, 305-353, South Korea
[*pilhan.kim@kaist.ac.kr](mailto:pilhan.kim@kaist.ac.kr)

Abstract: The recent development of THz sources in a wide range of THz frequencies and power levels has led to greatly increased interest in potential biomedical applications such as cancer and burn wound diagnosis. However, despite its importance in realizing THz wave based applications, our knowledge of how THz wave irradiation can affect a live tissue at the cellular level is very limited. In this study, an acute inflammatory response caused by pulsed THz wave irradiation on the skin of a live mouse was analyzed at the cellular level using intravital laser-scanning confocal microscopy. Pulsed THz wave (2.7 THz, 4 μ s pulsewidth, 61.4 μ J per pulse, 3Hz repetition), generated using compact FEL, was used to irradiate an anesthetized mouse's ear skin with an average power of 260 mW/cm² for 30 minutes using a high-precision focused THz wave irradiation setup. In contrast to *in vitro* analysis using cultured cells at similar power levels of CW THz wave irradiation, no temperature change at the surface of the ear skin was observed when skin was examined with an IR camera. To monitor any potential inflammatory response, resident neutrophils in the same area of ear skin were repeatedly visualized before and after THz wave irradiation using a custom-built laser-scanning confocal microscopy system optimized for *in vivo* visualization. While non-irradiated control skin area showed no changes in the number of resident neutrophils, a massive recruitment of newly infiltrated neutrophils was observed in the THz wave irradiated skin area after 6 hours, which suggests an induction of acute inflammatory response by the pulsed THz wave irradiation on the skin via a non-thermal process.

©2014 Optical Society of America

OCIS codes: (170.0170) Medical optics and biotechnology; (170.6795) Terahertz imaging; (000.1430) Biology and medicine; (170.1790) Confocal microscopy; (170.6930) Tissue.

References and links

1. P. H. Siegel, "Terahertz technology," *IEEE Trans. Microw. Theory Tech.* **50**(3), 910–928 (2002).
2. M. Tonouchi, "Cutting-edge terahertz technology," *Nat. Photonics* **1**(2), 97–105 (2007).
3. Y.-S. Lee, *Principles of Terahertz Science and Technology*, (Springer, 2008), Chap. 3.
4. P. Shumyatsky and R. R. Alfano, "Terahertz sources," *J. Biomed. Opt.* **16**(3), 033001 (2011).
5. P. H. Siegel, "Terahertz technology in biology and medicine," *IEEE Trans. Microw. Theory Tech.* **52**(10), 2438–2447 (2004).
6. A. R. Orlando and G. P. Gallerano, "Terahertz Radiation Effects and Biological Applications," *J. Infrared Millim. Terahertz Waves* **30**, 1308–1318 (2009).
7. G. J. Wilmink and J. E. Grundt, "Invited Review Article: Current State of Research on Biological Effects of Terahertz Radiation," *J. Infrared Millim. Terahertz Waves* **32**(10), 1074–1122 (2011).
8. E. P. Parrott, S. M. Sy, T. Blu, V. P. Wallace, and E. Pickwell-Macpherson, "Terahertz pulsed imaging in vivo: measurements and processing methods," *J. Biomed. Opt.* **16**(10), 106010 (2011).

9. R. M. Woodward, V. P. Wallace, D. D. Arnone, E. H. Linfield, and M. Pepper, "Terahertz pulsed imaging of skin cancer in the time and frequency domain," *J. Biol. Phys.* **29**(2/3), 257–259 (2003).
10. C. S. Joseph, R. Patel, V. A. Neel, R. H. Giles, and A. N. Yaroslavsky, "Imaging of ex vivo nonmelanoma skin cancers in the optical and terahertz spectral regions Optical and Terahertz skin cancers imaging," *J. Biophotonics* (2012).
11. A. J. Fitzgerald, V. P. Wallace, M. Jimenez-Linan, L. Bobrow, R. J. Pye, A. D. Purushotham, and D. D. Arnone, "Terahertz pulsed imaging of human breast tumors," *Radiology* **239**(2), 533–540 (2006).
12. H. Chen, T. H. Chen, T. F. Tseng, J. T. Lu, C. C. Kuo, S. C. Fu, W. J. Lee, Y. F. Tsai, Y. Y. Huang, E. Y. Chuang, Y. J. Hwang, and C. K. Sun, "High-sensitivity in vivo THz transmission imaging of early human breast cancer in a subcutaneous xenograft mouse model," *Opt. Express* **19**(22), 21552–21562 (2011).
13. H. Chen, W. J. Lee, H. Y. Huang, C. M. Chiu, Y. F. Tsai, T. F. Tseng, J. T. Lu, W. L. Lai, and C. K. Sun, "Performance of THz fiber-scanning near-field microscopy to diagnose breast tumors," *Opt. Express* **19**(20), 19523–19531 (2011).
14. A. J. Fitzgerald, S. Pinder, A. D. Purushotham, P. O'Kelly, P. C. Ashworth, and V. P. Wallace, "Classification of terahertz-pulsed imaging data from excised breast tissue," *J. Biomed. Opt.* **17**(1), 016005 (2012).
15. P. Doradla, K. Alavi, C. Joseph, and R. Giles, "Detection of colon cancer by continuous-wave terahertz polarization imaging technique," *J. Biomed. Opt.* **18**(9), 090504 (2013).
16. P. Tewari, C. P. Kealey, D. B. Bennett, N. Bajwa, K. S. Barnett, R. S. Singh, M. O. Culjat, A. Stojadinovic, W. S. Grundfest, and Z. D. Taylor, "In vivo terahertz imaging of rat skin burns," *J. Biomed. Opt.* **17**(4), 040503 (2012).
17. M. H. Arbab, D. P. Winebrenner, T. C. Dickey, A. T. Chen, M. B. Klein, and P. D. Mourad, "Terahertz spectroscopy for the assessment of burn injuries in vivo," *J. Biomed. Opt.* **18**(7), 077004 (2013).
18. D. B. Bennett, Z. D. Taylor, P. Tewari, R. S. Singh, M. O. Culjat, W. S. Grundfest, D. J. Sassoon, R. D. Johnson, J. P. Hubschman, and E. R. Brown, "Terahertz sensing in corneal tissues," *J. Biomed. Opt.* **16**(5), 057003 (2011).
19. D. Bennett, Z. Taylor, P. Tewari, S. Sung, A. Maccabi, R. Singh, M. Culjat, W. Grundfest, J. P. Hubschman, and E. Brown, "Assessment of corneal hydration sensing in the terahertz band: in vivo results at 100 GHz," *J. Biomed. Opt.* **17**(9), 097008 (2012).
20. K. Jeong, Y. M. Huh, S. H. Kim, Y. Park, J. H. Son, S. J. Oh, and J. S. Suh, "Characterization of blood using terahertz waves," *J. Biomed. Opt.* **18**(10), 107008 (2013).
21. Y. B. Ji, E. S. Lee, S. H. Kim, J. H. Son, and T. I. Jeon, "A miniaturized fiber-coupled terahertz endoscope system," *Opt. Express* **17**(19), 17082–17087 (2009).
22. K. W. Kim, K. S. Kim, H. Kim, S. H. Lee, J. H. Park, J. H. Han, S. H. Seok, J. Park, Y. Choi, Y. I. Kim, J. K. Han, and J. H. Son, "Terahertz dynamic imaging of skin drug absorption," *Opt. Express* **20**(9), 9476–9484 (2012).
23. I. Eehchgadda, J. A. Grundt, M. Tarango, B. L. Ibey, T. Tongue, M. Liang, H. Xin, and G. J. Wilmink, "Using a portable terahertz spectrometer to measure the optical properties of in vivo human skin," *J. Biomed. Opt.* **18**(12), 120503 (2013).
24. D. Crawley, C. Longbottom, V. P. Wallace, B. Cole, D. Arnone, and M. Pepper, "Three-dimensional terahertz pulse imaging of dental tissue," *J. Biomed. Opt.* **8**(2), 303–307 (2003).
25. N. Bourne, R. H. Clothier, M. D'Arienzo, and P. Harrison, "The effects of terahertz radiation on human keratinocyte primary cultures and neural cell cultures," *Altern. Lab. Anim.* **36**(6), 667–684 (2008).
26. M. R. Scarfi, M. Romanò, R. Di Pietro, O. Zeni, A. Doria, G. P. Gallerano, E. Giovenale, G. Messina, A. Lai, G. Campurra, D. Coniglio, and M. D'Arienzo, "THz exposure of whole blood for the study of biological effects on human lymphocytes," *J. Biol. Phys.* **29**(2/3), 171–176 (2003).
27. V. I. Fedorov, A. G. Khamoyan, E. Y. Shevela, and E. R. Chernykh, "Investigation of possibility of submillimeter laser using as instrument for diagnostics in medicine," *Proc. SPIE* **6734**, 673404 (2007).
28. G. J. Wilmink, B. D. Rivest, B. L. Ibey, C. L. Roth, J. Bernhard, and W. P. Roach, "Quantitative investigation of the bioeffects associated with terahertz radiation," *Proc. SPIE* **7562**, 75620L (2010).
29. G. J. Wilmink, B. D. Rivest, C. C. Roth, B. L. Ibey, J. A. Payne, L. X. Cundin, J. E. Grundt, X. Peralta, D. G. Mixon, and W. P. Roach, "In Vitro Investigation of the Biological Effects Associated With Human Dermal Fibroblasts Exposed to 2.52 THz Radiation," *Lasers Surg. Med.* **43**(2), 152–163 (2011).
30. G. J. Wilmink, B. L. Ibey, C. L. Roth, R. L. Vincelette, B. D. Rivest, C. B. Horn, J. Bernhard, D. Roberson, and W. P. Roach, "Determination of death thresholds and identification of terahertz (THz)-specific gene expression signatures," *Proc. SPIE* **7562**, 75620K (2010).
31. V. F. Kirichuk, N. V. Efimova, and E. V. Andronov, "Effect of high power terahertz irradiation on platelet aggregation and behavioral reactions of albino rats," *Bull. Exp. Biol. Med.* **148**(5), 746–749 (2009).
32. V. F. Kirichuk and A. A. Tsymbal, "Use of Terahertz Electromagnetic Waves for Correcting the Hemostasis Functions," *Med. Tekh.* **44**(1), 12–16 (2010).
33. N. P. Bondar, I. L. Kovalenko, D. F. Avgustinovich, A. G. Khamoyan, and N. N. Kudryavtseva, "Behavioral effect of terahertz waves in male mice," *Bull. Exp. Biol. Med.* **145**(4), 401–405 (2008).
34. K. T. Kim, J. Park, S. J. Jo, S. Jung, O. S. Kwon, G. P. Gallerano, W. Y. Park, and G. S. Park, "High-power femtosecond-terahertz pulse induces a wound response in mouse skin," *Sci. Rep.* **3**, 2296 (2013).
35. P. Kim, E. Chung, H. Yamashita, K. E. Hung, A. Mizoguchi, R. Kucherlapati, D. Fukumura, R. K. Jain, and S. H. Yun, "In vivo wide-area cellular imaging by side-view endomicroscopy," *Nat. Methods* **7**(4), 303–305 (2010).
36. K. Choe, Y. Hwang, H. Seo, and P. Kim, "In vivo high spatiotemporal resolution visualization of circulating T lymphocytes in high endothelial venules of lymph nodes," *J. Biomed. Opt.* **18**(3), 036005 (2013).

37. Y. U. Jeong, B. C. Lee, S. K. Kim, S. O. Cho, B. H. Cha, J. Lee, G. M. Kazakevitch, P. D. Vobly, N. G. Gavrilov, V. V. Kubarev, and G. N. Kulipanov, "First lasing of the KAERI compact far-infrared free-electron laser driven by a magnetron-based microtron," *Nucl. Instrum. Meth. A* **475**(1-3), 47–50 (2001).
38. Y. U. Jeong, G. M. Kazakevitch, B. C. Lee, S. O. Cho, J. Yoo, N. G. Gavrilov, and V. V. Kubarev, "Upgrade of a compact FIR FEL driven by a magnetron-based microtron for the wavelength range of 100-300 μm ," *Nucl. Instrum. Meth. A* **507**(1-2), 125–128 (2003).
39. E. Y. Chiang, A. Hidalgo, J. S. Chang, and P. S. Frenette, "Imaging receptor microdomains on leukocyte subsets in live mice," *Nat. Methods* **4**(3), 219–222 (2007).
40. M. H. Kim, W. Liu, D. L. Borjesson, F. R. Curry, L. S. Miller, A. L. Cheung, F. T. Liu, R. R. Isseroff, and S. I. Simon, "Dynamics of neutrophil infiltration during cutaneous wound healing and infection using fluorescence imaging," *J. Invest. Dermatol.* **128**(7), 1812–1820 (2008).
41. T. Motoike, S. Loughna, E. Perens, B. L. Roman, W. Liao, T. C. Chau, C. D. Richardson, T. Kawate, J. Kuno, B. M. Weinstein, D. Y. R. Stainier, and T. N. Sato, "Universal GFP reporter for the study of vascular development," *Genesis* **28**(2), 75–81 (2000).
42. S. Holzmann, C. H. Tripp, M. Schmuth, K. Janke, F. Koch, S. Saeland, P. Stoitzner, and N. Romani, "A model system using tape stripping for characterization of langerhans cell-precursors in vivo," *J. Invest. Dermatol.* **122**(5), 1165–1174 (2004).

1. Introduction

The Terahertz (THz) region of the electromagnetic waves is typically defined as the frequency region ranging from 0.1 to 10 THz. Historically, the THz region has been underused due to the limited availability of sources and detectors, in comparison to the neighboring optical and microwave regions, which leads researchers to refer to this region sometimes as "the Terahertz Gap." However, the recent development of various THz sources in a wide range of THz frequencies and power levels in both CW and pulsed form [1–4] has greatly increased scientific interest in the novel use of THz waves. Especially, even though the strong attenuation of THz by water might be a disadvantage for some biological uses, the unique characteristics of photons in the THz region, such as their unique spectral sensitivity to molecular dynamics, non-ionizing low photon energy, and strong interaction with water can provide new opportunities for various biomedical applications [5–8]. For example, there have been several reports about using THz waves for the diagnosis of many types of cancer, including skin cancer [9, 10], breast cancer [11–14], colon cancer [15]; THz waves have also been used to determine the degree classification of burn wounds [16, 17], and to characterize cornea [18, 19], blood [20], skin [21–23] and dental tissues [24]. Although these studies have successfully demonstrated the great potential of THz waves as a new window to examine biological samples for clinical application, our knowledge about the potential effects of THz wave irradiation on a live tissue at the cellular level is still very limited.

Recent *in vitro* studies using cultured cell have reported diverse cellular level effects induced by THz wave irradiation depending on cell type and exposure parameters (frequency, power, and duration). Normal human keratinocytes (NHK) showed no alteration in cellular viability, differentiation, or membrane permeability after pulsed THz wave (0.14-0.15THz) irradiation for as long as 24 hours with peak power of 62 mW/cm^2 [25]. Human lymphocytes showed no changes due to pulsed THz wave irradiation (0.12-0.13 THz) for 20 minutes at low average power of 1 mW/cm^2 [26]. On the other hand, an increased cell proliferation and DNA synthesis accompanied, by a significant level of cell death (38%), were observed after CW THz wave (3.68 THz) irradiation for 90 minutes with average power of 20 mW/cm^2 [27]. Recent studies conducted by the AFRL (Air Force Research Laboratory) demonstrated increased level of stress proteins and cell death in human dermal fibroblasts after exposure to CW THz wave (2.52 THz) irradiation for 40-80 minutes with average power of 81-227 mW/cm^2 ; changes were thought to be due mostly to photothermal effects [28–30].

Although these *in vitro* studies have provided valuable information about and insights into THz wave irradiation induced effects at the cellular level, *in vivo* studies using live animal models are critically needed to reveal the potentially complex cellular response of live tissue involving various types of tissue resident cells and physiological systems. Yet, only a handful of reports about the *in vivo* effects of THz wave irradiation on live animals, especially mammalian models such as mice and rats, have been reported [31–34]. Enhanced platelet aggregation and behavioral changes such as depression were reported in rat model after CW

THz wave (0.15 THz) irradiation for 60 minutes with average power of 3 mW/cm² [31]. Normalization of hemocoagulation and fibrinolysis were reported in rat model after CW THz wave (0.129 THz) irradiation for 30 minutes with average power of 0.1 mW/cm² [32]. In mouse model, an increased level of anxiety was revealed by behavioral assessment after CW THz wave (3.6 THz) irradiation for 30 minutes with average power of 23.6 mW/cm² [33].

As can be seen, despite their critical significance in implementing THz wave based biomedical applications, the short- and long-term cellular level effects of single or multiple THz wave irradiation on live animals *in vivo* are mostly unknown. In this study, we analyzed cellular level inflammatory response after pulsed THz wave irradiation in live mouse model *in vivo* using a custom-built laser-scanning confocal microscopy system reported previously [35, 36]. Pulsed THz wave (2.7 THz, 4 μs pulsewidth, 61.4 μJ per pulse, 3 Hz repetition) generated from a compact free-electron laser (FEL) implemented at the Korea Atomic Energy Research Institute (KAERI) [37, 38] was used to irradiate the ear skin of a live anesthetized mouse for 30 minutes. By using a concave mirror and high-precision focused THz wave irradiation setup, the pulsed THz wave was focused to form a 300 μm diameter spot which is very close to the diffraction limit. Average power density is 260 mW/cm². Interestingly, in contrast to previous *in vitro* studies using cultured cells at similar power levels of the CW THz waves [28], no temperature change at the surface of the ear skin was observed by the IR camera; this could be due to the protective epidermal layer, composed by keratinocytes, and the bulky dermal and subcutaneous tissues, with physiological blood circulation providing efficient heat dissipation. In addition, no visible changes of skin in terms of color or texture were observed after the THz wave irradiation.

To analyze the cellular level inflammatory response, potentially induced by THz wave irradiation, the number and distribution of neutrophils in the ear skin were monitored *in vivo* using a custom-built laser-scanning confocal microscopy system. As neutrophils are the first responders among many subtypes of immune cells, and because they can rapidly migrate to an inflammation site, newly infiltrating neutrophils are a clear marker of acute inflammatory response. To image neutrophils *in vivo*, anti-Gr-1 antibody conjugated with a red fluorophore, Alexa 647, was intravenously injected at 3 hours prior to imaging; this fluorophore fluorescently labeled the neutrophils in a systemic manner [39, 40]. For the repetitive imaging of the same skin area before and after THz wave irradiation, we identified a distinctive blood vessel pattern in the ear skin as a landmark using a genetically engineered mouse expressing green fluorescence protein (GFP) at the blood vessel wall under the control of a Tie2-promotor [41]. While the non-irradiated control skin area showed no changes in the number and distribution of neutrophils, a massive recruitment of newly infiltrated neutrophils was observed in the THz wave irradiated skin area after 8 hours. Histological analysis by Hematoxylin and Eosin (H&E) staining of irradiated and non-irradiated skin areas also revealed increased levels of leukocyte infiltration. These observations suggest that an acute inflammatory response can be induced *in vivo* by intensive pulsed THz wave irradiation on the skin via a non-thermal process.

2. Experimental setup and methods

2.1 THz wave generation and irradiation setup

Figure 1(a) shows the custom-built THz wave generation and irradiation setup implemented at the Korea Atomic Energy Research Institute (KAERI). A compact far infrared (FIR) free-electron laser (FEL) driven by a microtron was used to generate a high power THz wave pulse train at a frequency of 2.7 THz with 3 Hz repetition rate and 4 μs pulsewidth. The output FIR THz wave from the optical cavity mirror was transported to the irradiation setup through a vacuum tube integrated with relay optics. A mirror was placed in the vacuum tube to reflect the THz wave toward the irradiation setup through a polypropylene window. The transported THz wave has a small diverging angle of less than 5 mrad, with a spot size less than 40 mm in FWHM. 10 percent of the transported THz wave was extracted using a beam splitter in order to continuously monitor the power of the THz wave during irradiation. A

pyroelectric detector (P4-35, Molelectron) was used to measure the intensity of the THz wave. The THz wave was focused using an off-axis parabolic mirror (4 inch diameter, 150 mm focal length) onto a spot that was 300 μm in diameter. Average power density of the THz wave at the focus was 260 mW/cm^2 and the energy per pulse was 61.4 μJ . A visible laser beam at 640 nm, from a laser diode, was collinearly aligned with the THz wave using a dichroic beam splitter, which provided a visible guide for the coarse localization of the focal spot of the THz wave. Figure 1(b) provides a photograph of the THz wave irradiation setup with a live anesthetized mouse placed on an animal holder fixed to a motorized XYZ stage.

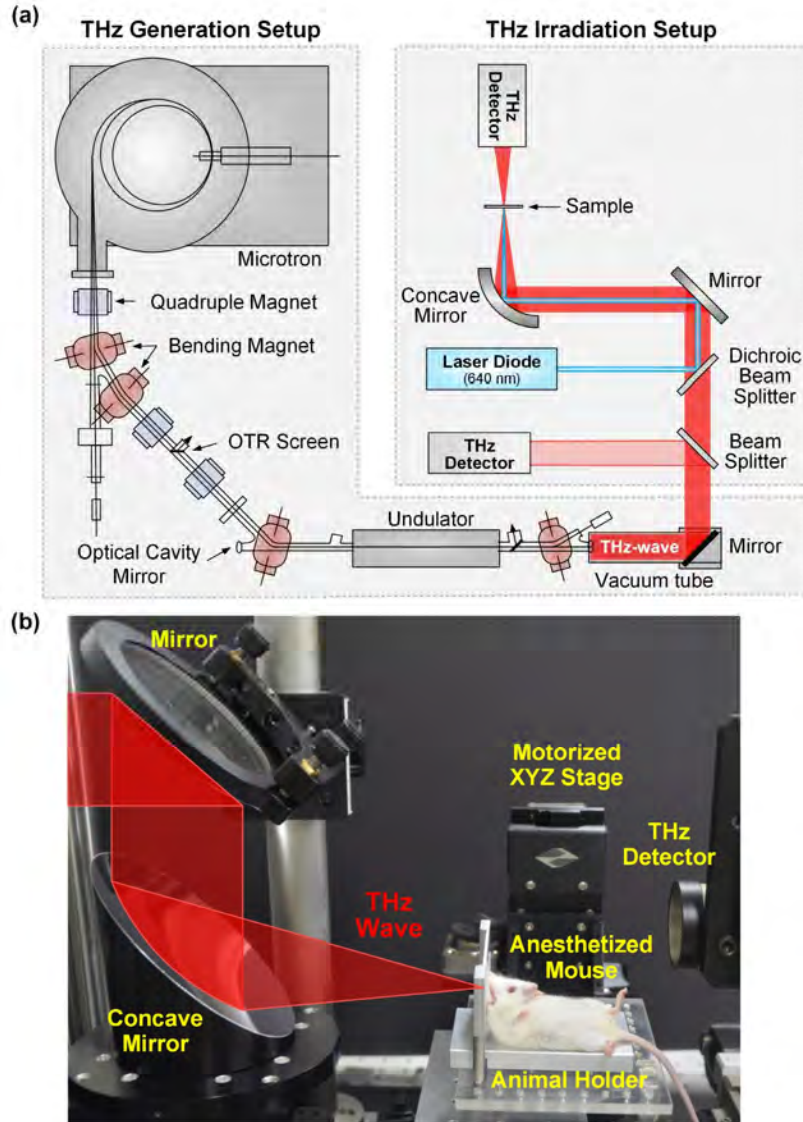


Fig. 1. THz wave generation and irradiation setup, (a) Schematics, (b) Photograph of the THz irradiation setup. A live anesthetized mouse was placed on the animal holder fixed to a motorized 3D stage.

2.2 Animal stage and focus mask for THz wave irradiation

In this study, a pulsed Terahertz wave (2.7 THz, 4 μs pulsewidth, 61.4 μJ per pulse, 3 Hz repetition rate) was tightly focused onto a small spot that was 300 μm in diameter in order to

provide a high irradiation power density of 260 mW/cm^2 . To precisely place the ear skin on the focused spot, we implemented a high precision focused THz wave irradiation setup, which is composed of a motorized XYZ stage (3DMS, Sutter instrument), a focus mask, and an animal holder, as shown in Fig. 2(a). The motorized stage provides 25 mm seamless translation in 3D with $1 \mu\text{m}$ step resolution. Animal holder was a custom designed aluminum block that has a rectangular shaped base and a vertically fixed plate with two holes (2 mm diameter). An anesthetized mouse can be placed on the base and the two ears can be attached to the vertical plate using adhesive tape. Position of each attached ear was adjusted to expose the center region by the hole on the vertical plate. Focus mask was an aluminum plate that has 4 inclined holes with diameters of 0.5 mm, 0.75 mm, 1 mm and 1.5 mm. Each hole on the focus mask was precisely made on the locations and those locations were exactly matched to the position of the hole on the vertical plate of the animal holder when they were placed in alignment with the focus mask holder, as shown in Fig. 2(b).

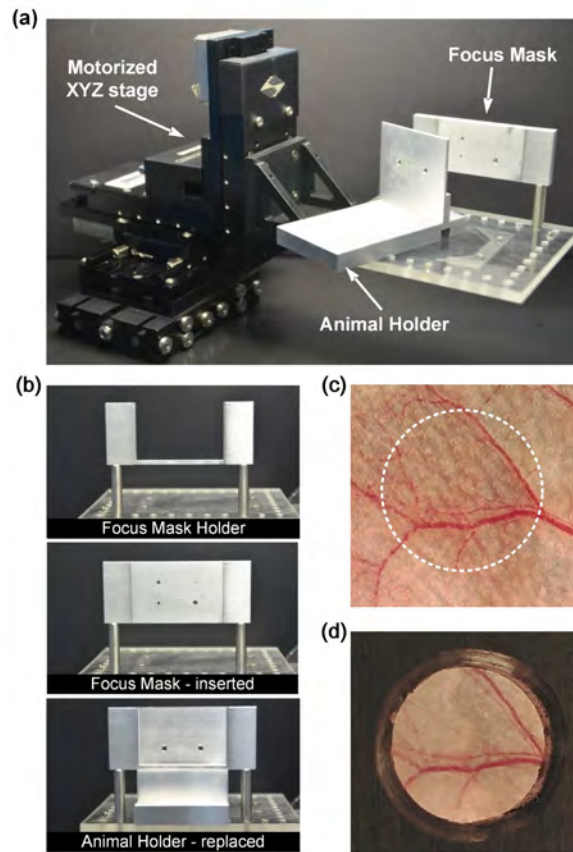


Fig. 2. High precision THz wave irradiation setup for mouse model, (a) Photograph of the setup, (b) Photographs of the focus mask holder (top), the focus mask holder inserted with the focus mask (middle), and the animal holder placed against the focus mask holder (bottom), (c) Microscopic picture of mouse ear skin showing distinctive blood vessel pattern identified for repetitive imaging analysis. (d) Microscopic picture of mouse ear skin attached against the vertical plate of the animal holder. Distinctive blood vessel pattern identical to the area in (c) marked by dotted circle was clearly visible through 2 mm diameter hole of the vertical plate of the animal holder.

To precisely irradiate the THz wave on the specific spot of ear skin, first, the focus mask was inserted into the focus mask holder, which was fixed on the acrylic plate attached to the motorized stage, as shown in Fig. 2(b). The exact position of the focused THz wave spot was determined in 3D by translating the focus mask with the motorized XYZ stage while

monitoring the THz wave power transmitted through the 1 mm diameter hole of the focus mask by the pyroelectric detector. Once the position of the focus of the THz wave was determined, the focus mask was removed from the focus mask holder. Then, the animal holder with an anesthetized mouse on it was carefully placed against the focus mask at the position where the 2 mm diameter hole on the vertical plate exposing the center of ear skin was aligned to the THz wave focal spot.

In this study, using intravital laser-scanning confocal microscopy, we imaged the same area of the ear skin before and after THz wave irradiation at the cellular level. To irradiate the THz wave on the exact area where the microscopic image was obtained, we identified a distinctive blood vessel pattern in the ear skin as a landmark. As the blood vessel on the ear skin is easily distinguishable and shows a unique pattern that does not rapidly change, its distinctive pattern can serve as an optimal landmark to locate the same skin area repeatedly. We preferentially pre-identified a large branching vessel, as shown in Fig. 2(c), as a skin area for repetitive imaging analysis: first, we performed imaging before the irradiation; this was followed by focused THz-wave irradiation, and then by a second imaging after the irradiation. The pre-identified blood vessel pattern can be easily located through the 2 mm diameter hole on the vertical plate of the animal holder, as shown in Fig. 2(d).

2.3 Intravital laser-scanning confocal microscopy system

For *in vivo* analysis of cellular level effects induced by THz wave irradiation on the skin of the live mouse, we utilized a custom-built laser-scanning confocal microscopy system that has been previously described [35, 36]. Figure 3 provides a schematic of the laser-scanning confocal microscopy system, which is capable of video-rate three-color fluorescence image acquisition. As excitation sources, three continuous-wave laser modules at 488 nm (MLD, Cobolt), 561 nm (Jive, Cobolt), and 640 nm (MLD, Cobolt) were used. All the laser beams were combined using dichroic beam splitters (DBS1; FF593-Di03, DBS2; FF520-Di02, Semrock); they were then delivered to a multi-edge dichroic beam splitter (DBS3; Di01-R405/488/561/635, Semrock). The collinearly aligned laser beams were scanned by a rotating 36 facet polygonal mirror (MC-5, aluminum coated, Lincoln Laser) and a galvanometer based scanning mirror (6230H, Cambridge Technology), which generated a two-dimensional raster scanning pattern. The scanning laser beams were delivered to the ear skin of the anesthetized mouse on the XYZ translation stage (3DMS, Sutter Instrument) through a commercial long working distance objective lens (LUCPlanFL, 20X, 0.45NA, Olympus), which provided a field of view of $500 \times 500 \mu\text{m}$. The three-color fluorescence signals from the sample were epi-detected by the objective lens and then the de-scanned fluorescence signals were separated from the excitation laser beam by a multi-edge dichroic beam splitter (DBS3). Then, the fluorescence signals were split into three colors (green, red, and far-red) by the dichroic beam splitters (DBS4; FF560-Di01, DBS5; FF649-Di01, Semrock) and band pass filters (BPF1; FF01-525/45, BPF2; FF01-600/37, BPF3; FF01-697/58, Semrock). Confocal pinholes were placed in front of each photomultiplier tube (PMT; R9110, Hamamatsu) used as fluorescence detectors. The electronic outputs from the PMTs were digitized using an 8-bit resolution 3-channel frame grabber (Solios, Matrox) with a sampling rate of 10 MHz for each channel. Three color images with sizes of 512×512 pixels were displayed and recorded in real time at a frame rate of 30 Hz by custom-written imaging software based on the Matrox Imaging Library (MIL9, Matrox).

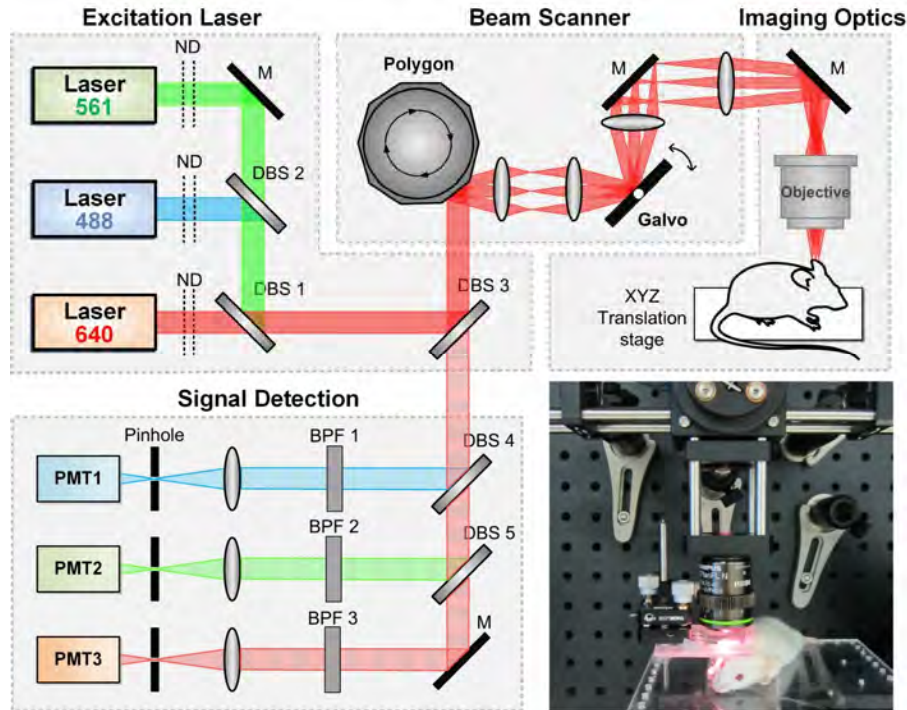


Fig. 3. Schematic of custom-built intravital laser-scanning confocal Microscopy: DBS, dichroic beam splitter; BPF, band pass filter; M, mirror; PMT, photomultiplier tube. Photograph shows the preparation of an anesthetized live mouse for ear skin imaging, in vivo.

2.4 Animal model

Mice were anesthetized by intramuscular injection of a mixture of zoletil (30 mg/kg) and xylazine (10 mg/kg). The ear skin was shaved using hair removal cream before the imaging and THz wave irradiation. During the entire experimental process, the body temperature was maintained at 36 °C with a mouse body temperature monitoring and homeothermic control system (PhysioSuite™, RightTemp, Kent Scientific). To fluorescently visualize the blood vessel pattern, a genetically engineered Tie2-eGFP mouse that endogenously expresses Green Fluorescent Protein (GFP) under the direction of the endothelial-specific receptor tyrosine kinase (Tie2) promoter was used. In the ear skin of the Tie2-eGFP mouse, the vascular endothelial cells of the blood vessels exclusively emitted bright green fluorescence signals when excited by the 488 nm laser beam.

3. Results

In this work, we focused on monitoring the inflammatory response in the skin after THz wave irradiation because this is the most common tissue reaction to external stimuli such as injury pathogens, and (potentially) electromagnetic waves. For example, in the skin, an inflammation can be induced by slight physical stimulation such as gentle tape stripping [42]; such a process would reveal a highly dynamic cellular level response on the microscopic scale, but there would be no visible change on the macroscopic scale. To monitor the inflammatory response at the cellular level, we visualized the behaviors of fluorescently labeled neutrophils in the skin of a live mouse after THz wave irradiation. It should be noted that neutrophils are first-responder immune cells that can rapidly migrate to inflammation sites within an hour via blood circulation. Neutrophils in the live mouse were fluorescently labeled in vivo by intravenously injecting 10 µg of anti-Gr-1 antibody (553122, BD) conjugated with a far-red fluorophore, Alexa Flour 647(A-20186, Invitrogen), at 12 hours

prior the first imaging before THz wave irradiation. Gr-1, granulocyte differentiation antigen 1, is a surface anchored protein that is highly expressed in mature granulocytes, mostly in neutrophils and in a small population of eosinophils. As eosinophils do not reside in the skin, we can presume that all of the fluorescently labeled cells observed in the skin are neutrophils.

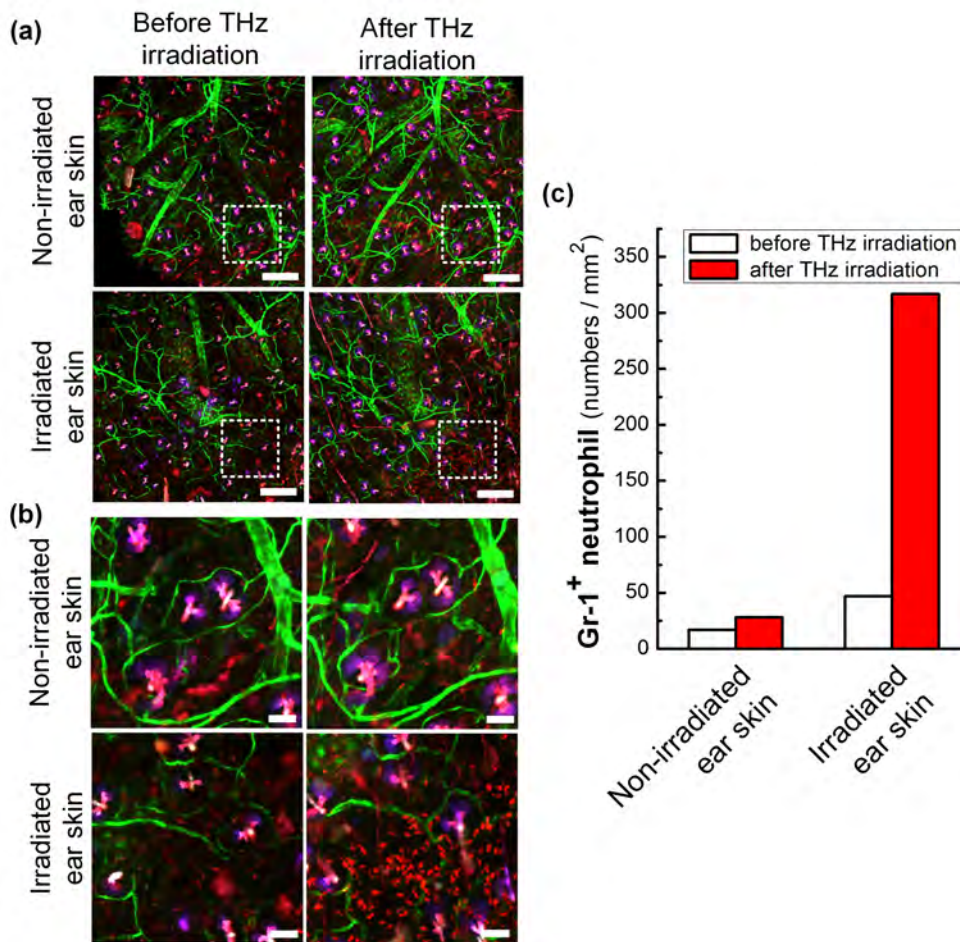


Fig. 4. (a) Distribution of neutrophils in the ear skin of a live mouse before and after THz wave irradiation, Gr-1 + neutrophil (red), Tie2 + blood vessel (green) and autofluorescent hair follicle (magenta). (b) Magnified images of the skin area marked by dotted line in (a). (c) Gr-1 + neutrophil density in the THz wave irradiated and non-irradiated skin. Scale bars are (a) 250 μ m and (b) 50 μ m, respectively.

As previously described in section 2.2, we imaged the same area of the ear skin at the cellular level repeatedly, before and after the THz wave irradiation, by using intravital laser-scanning confocal microscopy. A distinctive blood vessel pattern was identified as a landmark to locate the same skin area, as shown in Figs. 2(c) and 2(d). In a single mouse, only the right ear skin was irradiated by the THz wave for 30 minutes; as a control for comparison purposes the left ear skin was not irradiated. No differences between the irradiated and non-irradiated skin surfaces could be visually observed. Figure 4(a) provides the images of the ear skin, irradiated (right ear) and non-irradiated (left ear), obtained at 3 hours before and 6 hours after the THz wave irradiation. Blood vessel patterns in the dermal layer of each skin, revealed by green GFP fluorescence expressed in the vascular endothelial cells, are clearly visible. The dotted squares in Fig. 4(a) indicate the skin area shown in Fig. 4(b) with magnified view. As can be seen in the bottom panel in Fig. 4(b), we were able to

observe a significantly increased number of neutrophils in the THz wave irradiated skin area. Figure 4(c) shows the change in the density of neutrophils in the skin before and after THz wave irradiation; these values were quantified by using the ImageJ plug-in, Cell Counter. The neutrophil density in the irradiated skin was found to have dramatically increased (more than 6 times) after the THz wave irradiation, reaching a value of 317 cells per mm^2 , whereas the neutrophil density in the non-irradiated skin remained below 50 cells per mm^2 .



Fig. 5. Hematoxylin and Eosin (H&E)-stained microscope images from THz wave non-irradiated (left) and irradiated (right) ear skin harvested at 6 hours after THz wave irradiation. In the dermis, the increased number of inflammatory cells, neutrophils, was observed (arrowhead). In the epidermis, no definitely damaged cells or atypical keratinocytes were found. Also, no differences in the sebaceous gland or in the auricular cartilage were observed.

To further confirm the infiltration of neutrophils, we harvested the ear skin and performed conventional histological analysis. Figure 5 provides microscopic images obtained from the standard H&E stained ear skins with and without THz wave irradiation. As can be seen in the intravital microscopic imaging, an increased number of accumulated inflammatory cells, mostly neutrophils, were observed in the dermis as marked by the arrowhead. However, in the epidermis, the outermost layer of skin, no definitely damaged cells or atypical keratinocytes could be observed, which result matches well with our visual observation of the skin surface. Also, no differences in the sebaceous glands or in the auricular cartilage were found. These histological observations suggest the initiation of a relatively mild inflammatory response without any significant structural disruption.

4. Conclusion

In this study, we monitored cellular level inflammatory responses caused by pulsed THz irradiation in live mouse model *in vivo*. With a FEL based pulsed THz source, we irradiated anesthetized mouse ear skin using a pulsed THz wave (2.7 THz, 4 μs pulsewidth, 61.4 μJ per pulse, 3 Hz repetition) with an average power of 260 mW/cm^2 for 30 minutes. No temperature change at the surface of the irradiated mouse ear skin was detected by the IR camera. Utilizing a custom-built intravital laser-scanning confocal microscopy system, we visualized the same area of the ear skin repeatedly before and after THz wave irradiation in order to monitor the acute phase inflammatory response. Using a Tie2-eGFP mouse genetically engineered to express green fluorescence in the blood vessels, a distinctive blood vessel pattern of the ear skin was identified to locate the exact same skin area. As a first-responder cell for inflammation, skin-residing neutrophils, fluorescently labeled *in vivo* by an intravenous injection of anti-Gr-1 antibody conjugated with Alexa Fluor 647, were visualized and quantified; this process revealed a massive infiltration of Gr-1⁺ neutrophils to the THz wave irradiated skin area within 6 hours. Histological analysis based on standard H&E staining also confirmed an accumulation of inflammatory cells in the dermis of the irradiated skin with no observable changes in the skin structure. Collectively, these results suggest that an acute inflammatory response can be initiated without structural disruption in the skin by

pulsed THz wave irradiation; this is not a simple thermal effect due to the absorption of THz waves, like the case of the *in vitro* experiment. It also suggests that THz wave irradiation on live tissue in *in vivo* conditions can possibly trigger various unexpected dynamic responses that were not mimicked in the simplified *in vitro* conditions; this process needs to be investigated further and characterized for potential future biomedical applications.

Acknowledgments

This work was supported by the World Class Institute program (WCI 2011-001), the Engineering Research Center program (NRF-2009-0083512), the Global Frontier Project (NRF-M1AXA002-2012M3A6A4054261) of the National Research Foundation of Korea, and the Converging Research Center Program (2011K000864), funded by the Ministry of Science, ICT and Future Planning (MSIP); it was also supported by the Korea Healthcare Technology R&D Project, funded by Ministry of Health and Welfare (A103017).